



HAL
open science

Superimposition of maximal stress and necrosis areas at the top of the femoral head in hip aseptic osteonecrosis

J. -C. Escudier, M. Ollivier, M. Donnez, S. Parratte, P. Lafforgue, Jean-Noël Argenson

► To cite this version:

J. -C. Escudier, M. Ollivier, M. Donnez, S. Parratte, P. Lafforgue, et al.. Superimposition of maximal stress and necrosis areas at the top of the femoral head in hip aseptic osteonecrosis. *Orthopaedics & Traumatology: Surgery & Research*, 2018, 104 (3), pp.353-358. 10.1016/j.otsr.2018.01.008 . hal-01960510

HAL Id: hal-01960510

<https://hal.science/hal-01960510>

Submitted on 17 Apr 2019

HAL is a multi-disciplinary open access archive for the deposit and dissemination of scientific research documents, whether they are published or not. The documents may come from teaching and research institutions in France or abroad, or from public or private research centers.

L'archive ouverte pluridisciplinaire **HAL**, est destinée au dépôt et à la diffusion de documents scientifiques de niveau recherche, publiés ou non, émanant des établissements d'enseignement et de recherche français ou étrangers, des laboratoires publics ou privés.

Title: Superimposition of Maximal Stress and Necrosis Areas at the Top of the Femoral Head in Hip Aseptic Osteonecrosis

Author: J.-C. Escudier M. Ollivier M. Donnez S. Parratte P. Lafforgue J.-N. Argenson

Superimposition of Maximal Stress and Necrosis Areas at the Top of the Femoral Head in Hip Aseptic Osteonecrosis

J.-C. Escudier^{a,b}, M. Ollivier^{a,b,*}, M. Donnez^a, S. Parratte^{a,b}, P. Lafforgue^{a,c}, J.-N. Argenson^{a,b}

a Aix-Marseille University, CNRS, ISM UMR 7287, 13288, Marseille cedex 09, France.

b Institute of Movement and Locomotion, Department of Orthopedic Surgery and Traumatology, St. Marguerite Hospital, 270 Boulevard Sainte Marguerite, BP 29 13274 Marseille, France

c Institute of Movement and Locomotion, Department of Rheumatology, St. Marguerite Hospital, 270 Boulevard Sainte Marguerite, BP 29 13274 Marseille, France.

* Corresponding author: Matthieu Ollivier, Institute of Movement and Locomotion, Department of Orthopedic Surgery, St. Marguerite Hospital, 270 Boulevard Sainte Marguerite, BP 29 13274 Marseille, France

Phone: +33491745011, Fax: +33491745001,

Email: ollivier.mt@gmail.com

Abstract

Introduction

Recent reports described possible mechanical factors in the development and aggravation of osteonecrosis of the femoral head (OFH), but these have yet to be confirmed on dedicated mechanical study. We therefore developed a 3D finite element model based on in-vivo data from patients with incipient OFH, with a view to determining whether the necrosis area was superimposed on the maximal stress area on the femoral head.

Hypothesis

The location of the necrosis area is determined by stress on the femoral head.

Material and method

All patients from the rheumatology department with early stage OFH in our center were investigated. Analysis of CT scans showed stress distribution on the head by 3D finite elements models, enabling determination of necrosis volume within the maximal stress area and of the percentage intersection of necrosis within the stress area (%I n/s: necrosis volume in stress area divided by total stress area volume and multiplied by 100) and of stress within the necrosis area (%I s/n: stress volume in necrosis area divided by total necrosis area volume and multiplied by 100).

Results

Nineteen of the 161 patients assessed retrospectively for the period between 2006 and 2015 had incipient unilateral OFH, 10 of whom (4 right, 6 left) had CT scans of sufficient quality for inclusion. Mean age was 52 years (range, 37-81 years). Mean maximal stress was 1.63MPa, mean maximal exported stress volume was 2,236.9 mm³ and mean necrosis volume 6,291.1 mm³. Mean %I n/s was 83% and mean %I s/n 35%, with no significant differences according to gender, age, side or stress volume. There was a strong inverse correlation between necrosis volume and %I s/n ($R^2 = -0.92$) and a strong direct correlation between exported stress volume and %I s/n ($R^2 = 0.55$). %I s/n was greater in small necrosis (<7,000mm³).

Conclusion

OFH seems to develop within the maximal stress area on the femoral head. The present results need confirmation by larger-scale studies. We consider it essential to take account of these mechanical parameters to reduce failure rates in conservative treatment of OFH.

Level of evidence: IV. Case series

Key-words: osteonecrosis of the femoral head, necrosis area, maximal stress area, 3D finite element model

1. Introduction

Osteonecrosis of the femoral head (OFH) consists in impaired femoral head perfusion due to intravascular coagulation. Part of the subchondral bone supporting the joint surface becomes necrotic, causing collapse of the head and secondary osteoarthritis [1,2]. Many etiologies and risk factors have been identified, including chronic alcoholism, medication (including long-course corticosteroids, with dose-dependent risk), and metabolic diseases such as gout, hyperlipidemia and thrombophilia [2]. In 30% of cases, however, no etiology can be established, and the osteonecrosis is diagnosed as “idiopathic” [3,4].

The pathophysiology of osteonecrosis has been well described and is of vascular origin [1]. However, recent studies have shown a critical role of hip-joint loading, with anatomic variations in the development of OFH [2,5–9]. Stress location in the femoral head may thus account for necrosis location, in the summit [10,11]. However, this remains to be confirmed on mechanical study, and we therefore developed a 3D finite element model based on in-vivo data in patients with incipient OFH, to determine whether the necrosis area is superimposed on the area of maximal stress. The study hypothesis was that the location of the necrosis area is determined by mechanical factors: i.e., stress exerted by the weight of the pelvis over the femur.

2. Material and method

2.1 Patients

With institutional review board approval, a prospective data-base was used to analyze patients assessed for incipient OFH in our rheumatology department between 2006 and 2015. Patients were followed up on 3D imaging of the hip or pelvis to confirm diagnosis of osteonecrosis and assess extension.

Inclusion criteria comprised: early-stage OFH (stage 1 or 2 on Ficat's classification [12]: i.e., without head deformity), with hip or pelvis CT of sufficient quality for segmentation and meshing.

2.2 Methods

3D finite element models of the hip were constructed in 3 stages, using 3 different software applications.

a) Hip or pelvis CT scans were first imported to the Mimics 18™ segmentation package (Materialise, Leuven, Belgium). The software's semi-automatic tools created 3D models of the patient's pelvic and proximal femoral bone, and then created cartilage, unseen on CT, as an intermediate object by addition and subtraction operations on the pelvis and femur. The three resulting objects (pelvis, cartilage and femur) were first smoothed in Mimics to obtain an optimally homogeneous and anatomically faithful 3D structure (Figure 1). In parallel, the necrotic area of the head was located as the least dense area, and a corresponding 3D object was then created using the same software tools (Figure 2).

b) Pelvis, cartilage and femur were then exported to the 3-matic™ meshing application (Materialise, Leuven, Belgium). Each object was surface-meshed by triangles. Target size was 2.5 mm for the pelvis, 2 mm for the femur and 1.5 mm for the cartilage (Figure 3). Linear tetrahedral volume meshing was then applied.

c) The three meshed objects were then imported to Abaqus 14™ (Simulia, RI) to construct the finite element model. For modeling, each object was assumed to be homogeneously isotropic, with linear elastic behavior (Table 1). Various interactions between the objects were added. Pelvis and cartilage were taken to be mutually adherent (tie interaction). Between cartilage and femur, a friction interaction was modeled: normal behavior was linear, with 100 MPa/mm

penetration coefficient, and tangential behavior was frictionless. Pelvis and distal femoral surface were embedded; the femur was allowed only translation movements along the X and Y axes and rotation around Z. Uniform vertical 600N pressure was applied on the superior side of the pelvis, to simulate bipedal loading (Figure 4).

These successive manipulations enabled stress distribution on each femoral head to be obtained. The volume showing stress greater than 50% of the mean value for the femoral head was then exported to the initial 3D model. The intersection between necrosis volume and maximal stress volume was thus obtained and assessed as percentage necrosis/stress intersection (%I n/s) and as percentage stress/necrosis interaction (%I s/n) (Figure 5).

$\%I\ n/s = \text{necrosis volume within the maximal stress area} / \text{total necrosis volume} \times 100$

$\%I\ s/n = \text{stress volume within the necrosis area} / \text{total stress volume} \times 100$

2.3 Statistical analysis

Quantitative variables were expressed as mean±standard deviation, and qualitative variables as percentage; in view of the sample size, the non-parametric Wilcoxon test was used for quantitative variables and the Fisher test for qualitative variables. The significance threshold was set at $p = 0.05$. To limit disease progression related bias (volume effect), 2 subgroups were distinguished: small OFH (volume < 7,000 mm³) and large OFH (volume > 7,000mm³).

Intra- and inter-observer reproducibility was assessed by intra-class correlation coefficients for %I s/n and %I n/s by 2 different blinded observers delineating the necrosis area on 2 analyses at 7 days' interval, stress areas being determined automatically on the 2 analyses (Table 2).

3. Results

Only 19 of the 161 patients showed incipient (stage 1 or 2) OFH, and only 10 of these had imaging of sufficient quality for inclusion: 5 males and 5 females, with a mean age of 52 years (range, 37-81 years). OFH was unilateral in all cases: 4 right (40%) and 6 left (60%). Three patients had chronic alcohol abuse (30%), and 5 were taking long-course corticosteroids (50%); 1 had HIV infection (10%), and 1 had idiopathic OFH (10%).

Table 3 shows %I results in the overall series. Mean maximal stress was 1.628 nnnnnnnn MPa. Mean necrosis/maximal stress intersection volume was 1,837.2 nn409.1 mm³, mean %I n/s 82.1 nn14%, and mean %I s/n 35.3 nn13.1%.

There were no significant differences in %I s/n on univariate analysis according to gender ($p=0.7$), side ($p=0.8$), or etiology ($p=0.7$). Likewise, there were no significant differences in %I

n/s according to gender ($p=0.8$), side ($p=0.7$) or etiology ($p=0.8$) (Table 4). I.e., necrosis and stress area superimposition seemed independent of gender, side and etiology.

There was a strong inverse correlation between necrosis volume and %I s/n ($R^2 = -0.92$) and a strong direct correlation between exported stress volume and %I s/n ($R^2 = 0.55$): the greater the necrosis volume the smaller the %I s/n, and the greater the stress volume the greater the %I s/n. There were no correlations between %I n/s and stress or necrosis volume.

Five of the 10 OFHs were small ($< 7,000 \text{ mm}^3$) and 5 large ($> 7,000 \text{ mm}^3$). Table 3 shows subgroup analysis; there were no significant differences according to maximal stress ($p=0.682$), exported stress volume ($p=0.345$), or necrosis/stress area intersection or %I n/s ($p=0.087$). %I s/n was significantly greater in small OFH ($n=20$; $p=0.006$) (Table 5). Stress volume within necrosis volume seemed greater in small OFH.

4. Discussion

To our knowledge, this was the first study to investigate a possible relation between necrosis and stress area locations on 3D finite element analysis. Results seemed to show that the necrosis area is superimposed on the maximal stress area, with percentage necrosis/stress intersection exceeding 80% and percentage stress/necrosis intersection of 35%, especially in small OFH. This finding was independent of biometric factors (gender, etiology, side) and of the factors controlled for in the model (maximal stress, exported volume). An influence of the mechanical environment on the development and/or aggravation of OFH was supported by several previous experimental studies showing that femoral head loading influenced the development of OFH [6,7,13,14]. Kim et al. [6] reported a series of animal models of OFH and concluded that, in pigs with induced OFH, non-weight-bearing slowed the natural progression of osteonecrosis. In a recent study, Ollivier et al. [5] likewise found that OFH patients presented anatomic abnormalities liable to modify stress on the summit of the femoral head.

The present study has several limitations. Firstly, the design was single-center and retrospective, limiting extrapolation. Moreover, it was a preliminary study; only 10 scans were included in 3D analysis, which highlights two points: the difficulty of large-scale inclusion in this rare pathology, and the infraclinical progression and diagnostic nomadism of some patients who consult only after long disease progression and serious deterioration of bone tissue. The 3D finite element model is also debatable: it was not always possible to differentiate between cartilage of the head and of the labrum due to the pathology and to the poor resolution of CT without contrast enhancement. This led us to create an intermediate object to represent the cartilage; this compromise, however, has been validated in the recent literature on a similar subject [15]. We did not differentiate cortical and trabecular bone on Young's modulus or Poisson coefficient, assuming the bone to be smooth and homogeneous throughout, as it is difficult to reconstruct and model femoral trabecular bone, which differs between head, neck and trochanteric region, and as

the properties of necrotic trabecular bone have not been described. The present method was used in other 3D models of the hip [16,17]. The present mechanical model was, however, robust, including interactions between the objects (tie interaction between pelvis and cartilage, and linear friction between cartilage and femur) [15,18], and the permitted movements [17,18–20] and loads [20–23] validated in the literature. Moreover, it comprised 10 3D analyses, ensuring greater clinical relevance than models extrapolated from a single hip as in all other finite element modeling studies. Reconstructions were based on pathological femurs under normal therapeutic conditions rather than experimental conditions, further enhancing clinical relevance. And lastly, all patients had very early necrosis, without femoral deformity, thus providing “cleaner” models without the alterations in stress distribution associated with advanced necrosis.

The present mean maximal stress value on finite element analysis (1.63 MPa) was low in comparison to certain reported values, which range between 3 and 6 MPa [15,19,22,24,25]; this was due to greater pressure being applied directly on the femur in these studies (Table 6): these previous studies aimed to model forces passing through the hip during daily life activity, representing loading equivalent to 4 times the body-weight [22]. We chose to apply a 600N load, modeling standard bipedal weight-bearing, exerted vertically downward on the superior side of the pelvis, which seemed more physiological than force applied directly on the femur, as we sought to study stress transmitted from the pelvis to the femoral head; moreover, increasing the load would doubtless have increased the stress area, enhancing %I values but introducing a measurement bias similar to that we described in patients with large necrosis volume. Comparison between the present results and the literature is difficult, as previous studies focused rather on the optimal means of quantifying necrosis volume [23], the influence of necrosis volume on fracture risk [24], the impact of anatomic variants on OFH [2,5], or the effects of different treatments [23]. Anderson et al. [20] reported only contact areas ranging between 304.2 and 366.1 mm² in their finite element analysis. To our knowledge, the maximal stress volume on the femoral head has never been calculated or studied elsewhere, and nor has superimposition between necrosis and stress areas. This may explain the better results found with aggressive treatment of OFH such as femoral varization or rotation osteotomy [24–29] than with conservative treatments such as decompression [30,31] or stem-cell injection [32] that do not modify stress distribution on the head. This theory, however, would not be applicable to certain OFH etiologies such as sickle-cell disease, where the necrosis area is usually posterior [33].

5. Conclusion

The results of the present finite element model of OFH support the mechanical theory of the pathophysiology of osteonecrosis of the hip. Hip anatomy and biomechanics seem to play a non-negligible role in the genesis of OFH: in the present study, necrosis developed in the area of the femoral head in which stress was greatest, although no direct causal relation can be affirmed. These findings need confirmation in larger-scale multicenter studies using a finite element model even closer to clinical reality. It seems to us to be primordial to take these mechanical parameters into account to limit failure of conservative treatment of OFH.

Conflicts of interest: None of the authors have conflicts of interest to disclose in relation to the present study. Elsewhere, J.C. Escudier, M. Donnez, M. Ollivier and P. Lafforgue have no conflicts of interest to disclose, while S. Parratte is an education consultant for Zimmer, Arthrex and Adler, and J.N. Argenson is an education consultant for Zimmer and Symbios and receives royalties from Zimmer

References

- [1] Guerado E, Caso E. The physiopathology of avascular necrosis of the femoral head: an update. *Injury* 2016;47 Suppl 6:S16–26.
- [2] Fraitzl CR, Kappe T, Brugger A, Billich C, Reichel H. Reduced head-neck offset in nontraumatic osteonecrosis of the femoral head. *Arch Orthop Trauma Surg* 2013;133:1055–60.
- [3] Dudkiewicz I, Covo A, Salai M, Israeli A, Amit Y, Chechik A. Total hip arthroplasty after avascular necrosis of the femoral head: does etiology affect the results? *Arch Orthop Trauma Surg* 2004;124:82–5.
- [4] Assouline-Dayyan Y, Chang C, Greenspan A, Shoenfeld Y, Gershwin ME. Pathogenesis and natural history of osteonecrosis. *Semin Arthritis Rheum* 2002;32:94–124.
- [5] Ollivier M, Lunebourg A, Abdel MP, Parratte S, Argenson J-N. Anatomical Findings in Patients Undergoing Total Hip Arthroplasty for Idiopathic Femoral Head Osteonecrosis. *J Bone Joint Surg Am* 2016;98:672–6.
- [6] Kim HKW, Aruwajoye O, Stetler J, Stall A. Effects of non-weight-bearing on the immature femoral head following ischemic osteonecrosis: an experimental investigation in immature pigs. *J Bone Joint Surg Am* 2012;94:2228–37.
- [7] Nishimura Y. The role of mechanical stress on the femoral head in the occurrence of femoral head lesions in spontaneously hypertensive rats. *Nihon Seikeigeka Gakkai Zasshi* 1991;65:767–74.
- [8] Mankin HJ. The reaction of articular cartilage to injury and osteoarthritis (first of two parts). *N Engl J Med* 1974;291:1285–92..
- [9] Mankin HJ. The reaction of articular cartilage to injury and osteoarthritis (second of two parts). *N Engl J Med* 1974;291:1335–40.
- [10] Yang J-W, Koo KH, Lee MC, Yang P, Noh MD, Kim SY, et al. Mechanics of femoral head osteonecrosis using three-dimensional finite element method. *Arch Orthop Trauma Surg* 2002;122:88–92.

- [11] Kaushik AP, Das A, Cui Q. Osteonecrosis of the femoral head: An update in year 2012. *World J Orthop* 2012;3:49–57.
- [12] Ficat RP. Idiopathic bone necrosis of the femoral head. Early diagnosis and treatment. *J Bone Joint Surg Br* 1985;67:3–9.
- [13] Mihara K, Hirano T. Standing is a causative factor in osteonecrosis of the femoral head in growing rats. *J Pediatr Orthop* 1998;18:665–9.
- [14] Hungerford DS, Lennox DW. The importance of increased intraosseous pressure in the development of osteonecrosis of the femoral head: implications for treatment. *Orthop Clin North Am* 1985;16:635–54.
- [15] Sanchez Egea AJ, Valera M, Parraga Quiroga JM, Proubasta I, Noailly J, Lacroix D. Impact of hip anatomical variations on the cartilage stress: a finite element analysis towards the biomechanical exploration of the factors that may explain primary hip arthritis in morphologically normal subjects. *Clin Biomech Bristol Avon* 2014;29:444–50.
- [16] Anderson AE, Ellis BJ, Maas SA, Weiss JA. Effects of idealized joint geometry on finite element predictions of cartilage contact stresses in the hip. *J Biomech* 2010;43:1351–7.
- [17] Chen GX, Yang L, Li K, He R, Yang B, Zhan Y, et al. A Three-Dimensional Finite Element Model for Biomechanical Analysis of the Hip. *Cell Biochem Biophys* 2013;67:803–8.
- [19] Yoshida H, Faust A, Wilckens J, Kitagawa M, Fetto J, Chao EY-S. Three-dimensional dynamic hip contact area and pressure distribution during activities of daily living. *J Biomech* 2006;39:1996–2004.
- [20] Anderson AE, Ellis BJ, Maas SA, Peters CL, Weiss JA. Validation of Finite Element Predictions of Cartilage Contact Pressure in the Human Hip Joint. *J Biomech Eng* 2008;130:051008.
- [21] Grecu D, Puculev I, Negru M, Tarnita DN, Ionovici N, Dita R. Numerical simulations of the 3D virtual model of the human hip joint, using finite element method. *Rom J Morphol Embryol* 2010;51:151–5.
- [22] Recnik G, Kralj-Iglic V, Iglic A, Antolic V, Kramberger S, Vengust R. Higher peak contact hip stress predetermines the side of hip involved in idiopathic osteoarthritis. *Clin Biomech Bristol Avon* 2007;22:1119–24.
- [23] Bergmann G, Deuretzbacher G, Heller M, Graichen F, Rohlmann A, Strauss J, et al. Hip contact forces and gait patterns from routine activities. *J Biomech* 2001;34:859–71.
- [24] Genda E, Iwasaki N, Li G, MacWilliams BA, Barrance PJ, Chao EY. Normal hip joint contact pressure distribution in single-leg standing--effect of gender and anatomic parameters. *J Biomech* 2001;34:895–905.
- [25] Steinberg DR, Steinberg ME, Garino JP, Dalinka M, Udupa JK. Determining lesion size in osteonecrosis of the femoral head. *J Bone Joint Surg Am* 2006;88 Suppl 3:27–34.

- [26] Volokh KY, Yoshida H, Leali A, Fetto JF, Chao EYS. Prediction of femoral head collapse in osteonecrosis. *J Biomech Eng* 2006;128:467–70.
- [27] Baba T, Nozawa M, Homma Y, Ochi H, Ozaki Y, Watari T, et al. Long-term results of rotational acetabular osteotomy for osteonecrosis with collapse of the femoral head in young patients. *Arch Orthop Trauma Surg* 2017;137:925–31.
- [28] Yamamoto T, Motomura G, Karasuyama K, Nakashima Y, Doi T, Iwamoto Y. Results of the Sugioka transtrochanteric rotational osteotomy for osteonecrosis: Frequency and role of a defect of the quadratus femoris muscle in osteonecrosis progression. *Orthop Traumatol Surg Res* 2016;102:387-90.
- [29] Sugioka Y, Yamamoto T. Transtrochanteric posterior rotational osteotomy for osteonecrosis. *Clin Orthop Relat Res* 2008;466:1104–9.
- [30] Schneider W, Breitenseher M, Engel A, Knahr K, Plenck H, Hofmann S. The value of core decompression in treatment of femur head necrosis. *Orthopade* 2000;29:420–9.
- [31] Bellot F, Havet E, Gabrion A, Meunier W, Mertl P, de Lestang M. Core decompression of the femoral head for avascular necrosis. *Rev Chir Orthop* 2005;91:114–23.
- [32] Rosset P, Deschaseaux F, Layrolle P. Cell therapy for bone repair. *Orthop Traumatol Surg Res OTSR* 2014;100:S107–12.
- [33] Mukisi-Mukaza M, Saint Martin C, Etienne-Julan M, Donkerwolcke M, Burny ME, Burny F. Risk factors and impact of orthopaedic monitoring on the outcome of avascular necrosis of the femoral head in adults with sickle cell disease: 215 patients case study with control group. *Orthop Traumatol Surg Res* 2011;97:814–20.

FIGURE LEGENDS

Figure 1: Creation of objects (pelvis, cartilage and femur) smoothed under Mimics™ (Materialise, Leuven, Belgium) to obtain a 3D structure optimally homogeneous and faithful to patient anatomy.

Figure 2: Location and definition of necrosis area.

Figure 3: Surface-meshing by triangles. Element target size was 2.5 mm for the pelvis, 2 mm for the femur and 1.5 mm for the cartilage.

Figure 4: Application of uniform vertical downward 600N pressure on the superior side of the pelvis, to simulate bipedal loading.

Figure 5: Visualization of the intersection between necrosis and maximal stress volumes.

Table 1: Material properties used in finite element model

	Type of material	Young's modulus (MPa)	Poisson coefficient
Pelvis	Bone	10,000	0.3
Femur	Bone	10,000	0.3
Cartilage	Cartilage	10	0.4

Table 2: Intra- and inter-observer reproducibility was assessed by intra-class correlation coefficients (ICC) with 95% CI for %I s/n and %I n/s by 2 different blinded observers delineating the necrosis area on 2 analyses at 7 days' interval.

Intra-observer reproducibility	ICC	95% CI
Observer 1	0.95	0.89–0.99
Observer 2	0.91	0.85–0.97
Inter-observer reproducibility	0.89	0.84–0.94

Table 3: Analysis of superimposition in the overall series.

Patient	Ficat stage [12]	Max. stress (MPa)	Exported stress volume (mm ³)	Necrosis volume (mm ³)	Necrosis/stress intersection (mm ³)	%I s/n	%I n/s
1	1	1.48	1,652.4	3,038	1,510.1	50	91
2	2	0.93	3,064.2	7,213.5	2,524.3	35	82
3	2	1.38	2,645.7	3,423.7	1,823.3	53	69
4	1	1.18	2,580	2,961.7	1,501.9	51	58
5	1	3.09	2,019	13,947.5	1,792.5	13	89
6	2	1.12	2,350	7,849.8	2,274.5	29	97
7	2	1.56	2,356.5	8,635.3	2,036.9	24	86
8	2	1.89	2,103.1	7,789	2,082.7	27	99
9	2	2.13	1,858.4	5,196	1,696.7	33	91
10	1	1.52	1,739.5	2,856.1	1,129.1	40	65
Mean		1.628	2,236.8	6291.1	1,837.2	35	83
Standard deviation		0.624	446.474	3,535.961	409.097	13	14

%I n/s (percentage necrosis/stress intersection) = necrosis volume within maximal stress area / total necrosis volume x 100. **%I s/n** (percentage stress/necrosis intersection) = stress volume within necrosis area / total stress volume x 100.

	Maximal stress	Exported stress volume	Measured necrosis volume	%I s/n	%I n/s
Gender					
Male	1.61 ± 0.85	2,081.5±556.3	6,465.24 ± 4,722.5	35.6 ± 16.9	85.6 ± 14
Female	1.64 ± 0.39	2,392±480.6	6,116.9 ± 3,398.7	36.4 ± 10.19	82.80 ± 13.6
<i>p</i>	0.6	0.5	0.6	0.7	0.6
Side					
Left	1.74 ± 0.33	2,240.9±337.9	6,261.1 ± 2,391.4	35.2 ± 13	84.25 ± 12.68
Right	1.55 ± 0.78	2,234.2 ± 538.7	6,311.1 ± 4,367.2	36.3 ± 14.2	81.3 ± 15.51
<i>p</i>	0.6	0.7	0.8	0.8	0.7
Etiology					
Alcohol	1.99 ± 0.94	2,134.7 ± 464	6,742.4 ± 6,246.2	33.33 ± 20.4	77.33 ± 12.8
Corticosteroids	1.538 ± 0.52	2,392.4 ± 520.47	6,359.1 ± 1,463	34.51 ± 5.12	83.2 ± 7.3
Viral (n=1)	1.12	2,350	7,849.8	29	97
Idiopathic (n=1)	1.48	1,652.4	3,038	50	91
<i>p</i>	0.4	0.5	0.5	0.7	0.3

Table 4: Influence of confounding demographic and etiologic factors on endpoints.

%I n/s (percentage necrosis/stress intersection) = necrosis volume within maximal stress area / total necrosis volume x 100. **%I s/n** (percentage stress/necrosis intersection) = stress volume within necrosis area / total stress volume x 100.

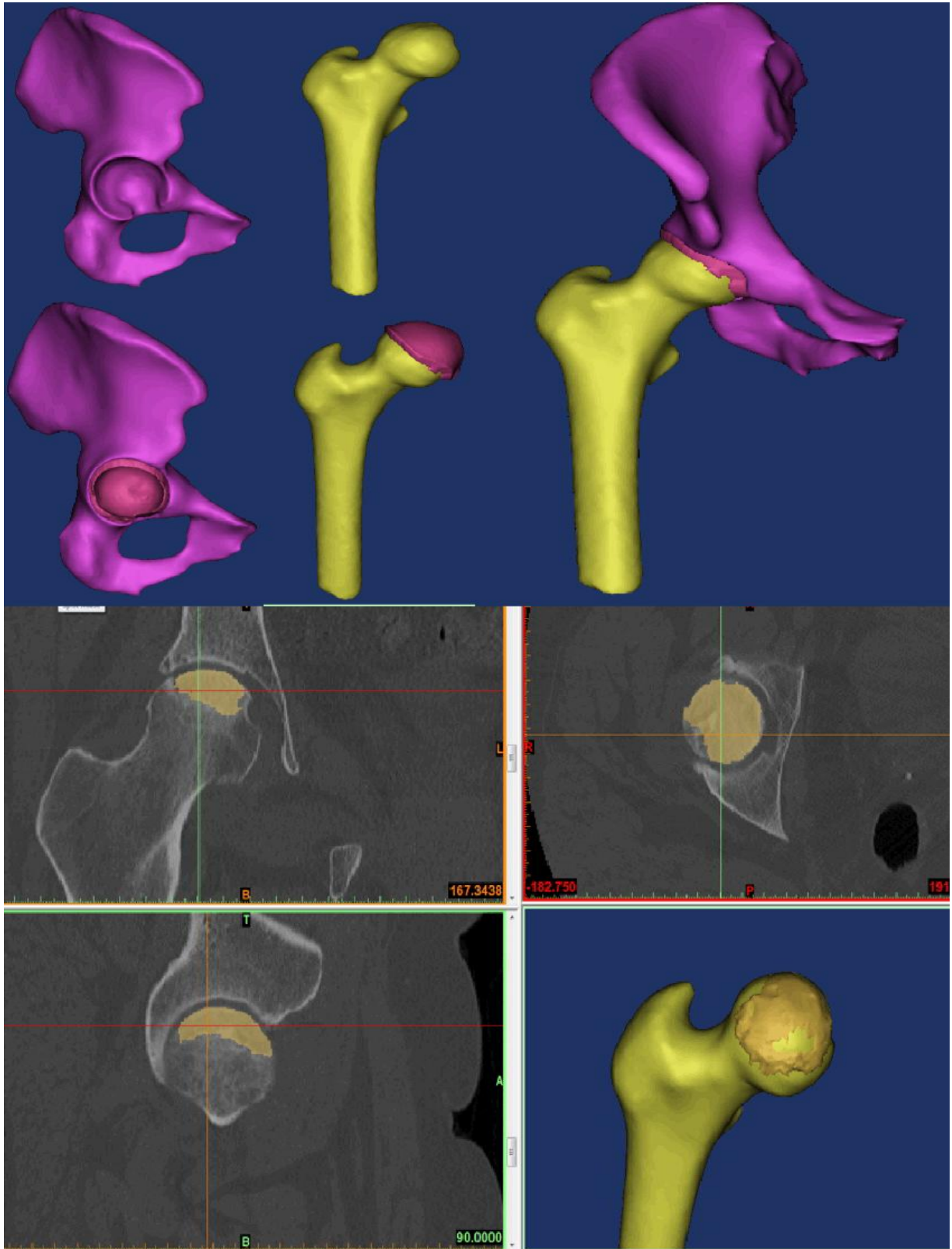
Table 5: Superimposition rate (mean±SD) by subgroup.

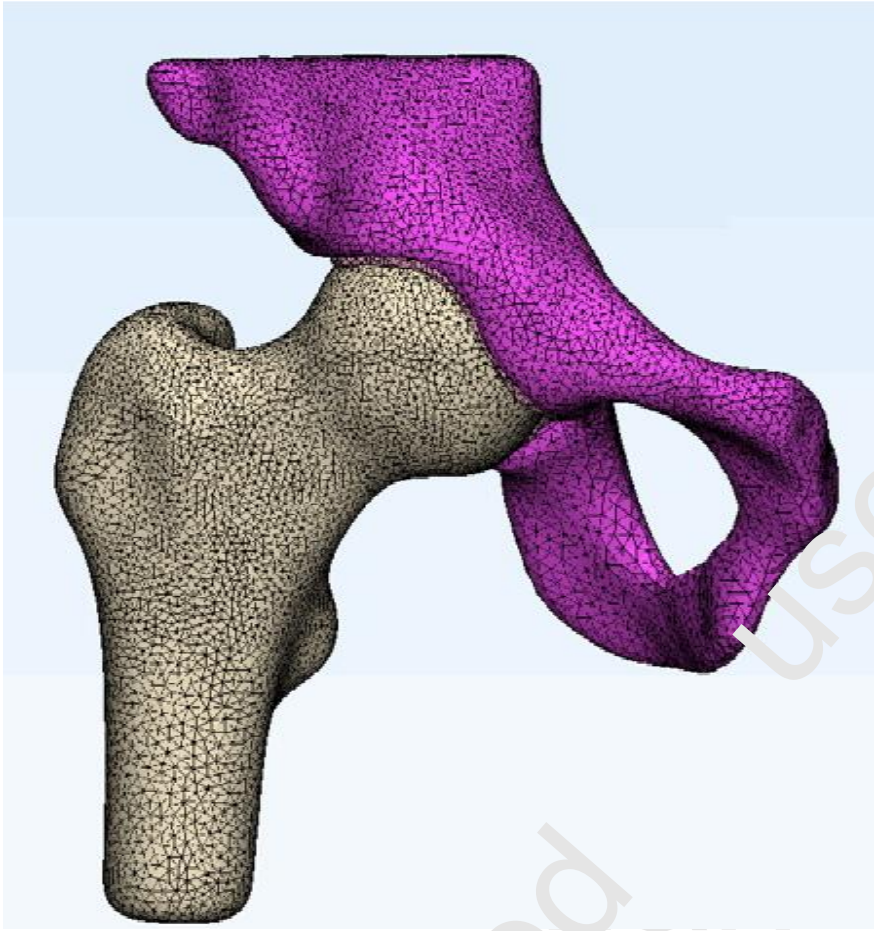
Subgroup	Maximal stress (MPa)	Exported stress volume (mm³)	Necrosis volume (mm³)	Necrosis/stress intersection (mm³)	%I s/n	%I n/s
Small necrosis	1.5 ± 0.4	2,095.2 ± 478.7	3,495.16 ± 974.8	1,532.2 ± 262.5	45 ± 10	75 ± 15
Large necrosis	1.7 ± 0.9	2,378.56 ± 411.3	9,087.02 ± 2,763	2,142.1 ± 274.1	25 ± 10	91 ± 7
p	0.682	0.345	0.008*	0.007*	0.006*	0.087

* p<0.05. **%I n/s** (percentage necrosis/stress intersection) = necrosis volume within maximal stress area / total necrosis volume x 100. **%I s/n** (percentage stress/necrosis intersection) = stress volume within necrosis area / total stress volume x 100.

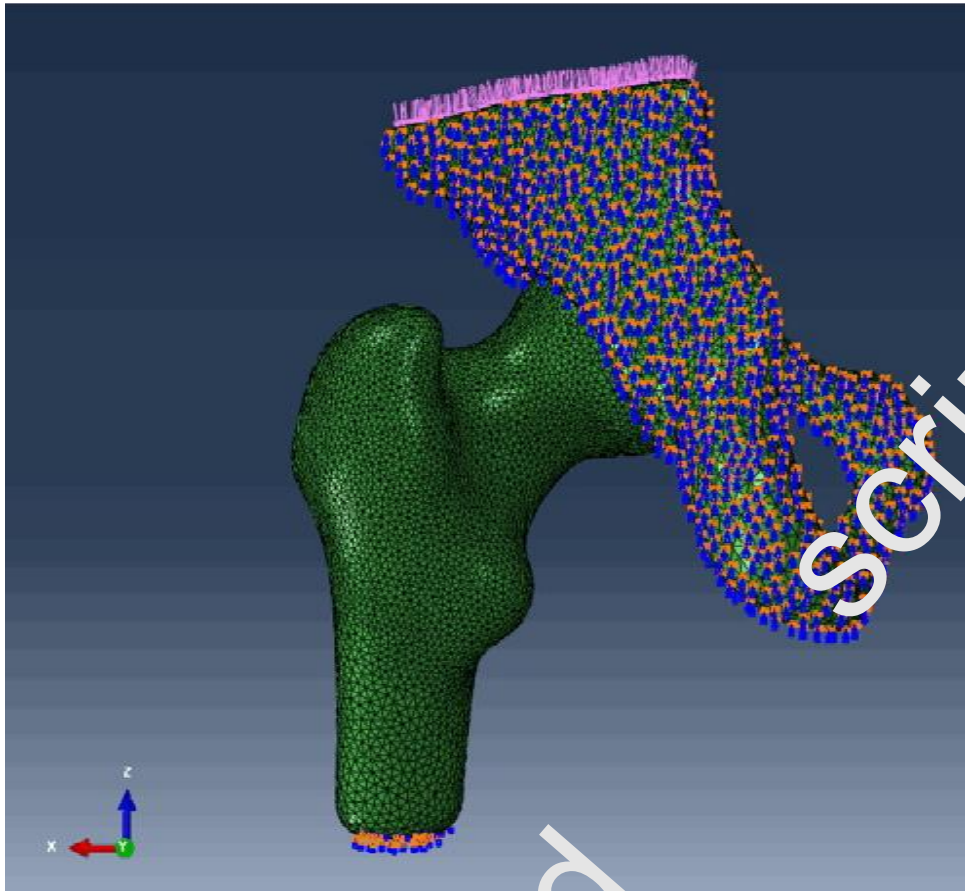
Table 6: Loading condition and related stresses in the current literature.

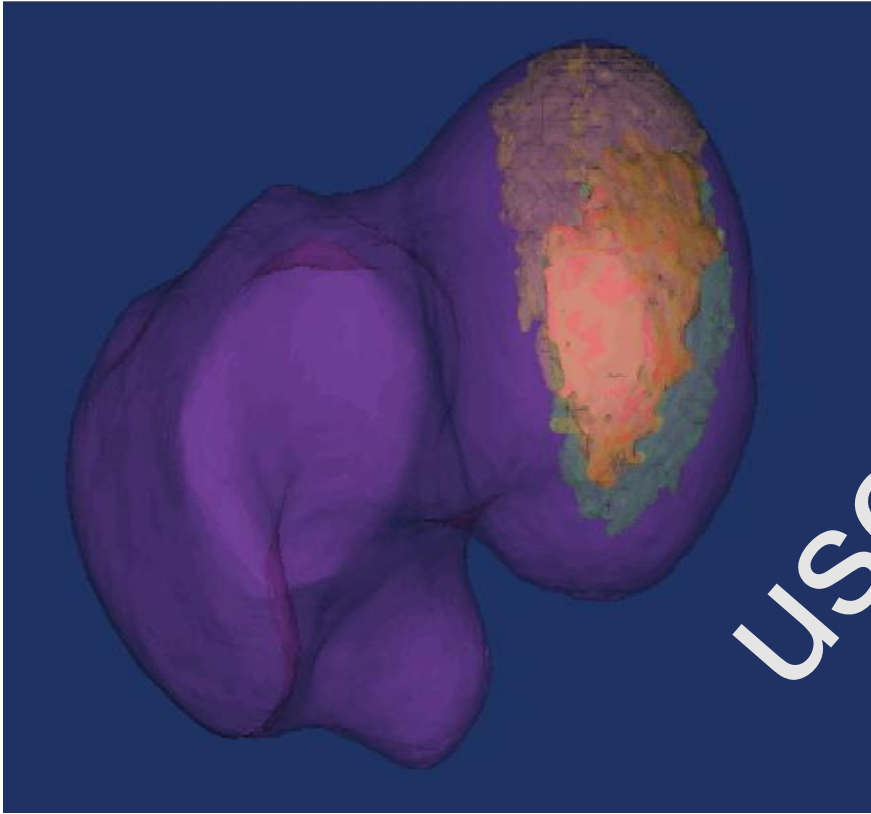
	Load (N)	Load location	Stress (MPa)
Present study	600	Pelvis	1.63
Chen et al. [17]	1,358	Femoral head	4.77
Anderson et al. [20]	2,000	Femoral head	4.4-5
Yang et al. [10]	3,000	Femoral head	-
Sanchez et al. [15]	550	Femoral head	2.5
Greco et al. [21]	500	Sacro-iliac	2.8
Genda et al. [24]	686	L5	1.67 females 1.38 males





Accepted Manuscript





Accepted Manuscript

uscript